Bulletin of the Seismological Society of America, Vol. 97, No. 2, pp. 545–556, April 2007, doi: 10.1785/0120060083

Seismic-Wave Attenuation and Source Excitation in La Paz–Los Cabos, Baja California Sur, Mexico

by Roberto Ortega and Mario González

Abstract We present results from a regional study of seismic-wave attenuation and source excitation from small-magnitude earthquakes recorded at distances from 6 to 180 km in the La Paz–Los Cabos region, at the south end of the Baja California Peninsula. Data were recorded using 32 strong-motion seismic stations from the La Paz network (LAP). A least-squares regression separating the excitation, site, and propagation effects was carried out. We performed the analyses in the time and frequency domains, and we compared these results with results from a coda-normalization method. The propagation term was parameterized to represent a geometrical spreading function and a frequency-dependent $Q(f)$ at a reference distance of 40 km. We estimated the regional attenuation by measuring the maximum amplitude of the *S* or *Lg* waves as a function of frequency, defining a continuous piecewise propagation term, $D(r, f)$, after separating the excitation and site terms. Our results show that the attenuation is lower than that of central or northern Mexico. Recorded data were of remarkably good quality despite the fact that the strong-motion network recorded only small earthquakes. Our best model is that of a quality factor of $Q(f) = 380f^{0.10}$ with a complex geometrical spreading function.

Introduction

The La Paz–Los Cabos region is located at the southernmost tip of the Baja California peninsula between 22°30′–25° N and 109°–111° W in the Gulf Extensional Province (Fig. 1). The Rivera triple junction is southeast of the study area, at the boundaries of the Pacific, North American, and Rivera tectonic plates. Therefore, the complex interaction of these plates should contribute to the transpeninsular fault systems in the La Paz–Los Cabos region. This is a seismically active region with little seismic history reported. On 30 June 1995 a moderate earthquake (M_S 6.2) and its principal aftershock (M_S 5.4) struck near the city of La Paz. Before 1995, two moderate events of M_S 5.6 and 5.0 occurred on 4 and 18 April 1969, respectively, east of Isla Cerralvo, and two events of M_S 5.3 occurred on 21 and 22 August 1969 offshore of Todos Santos (Molnar, 1973; Goff *et al.*, 1987; Munguía *et al.*, 1992). The Centro de Investigación Científica y de Educación Superior de Ensenada (CICESE) has deployed a digital strong-motion seismic network in the area since October 1998. During the past 7 years this network has been continuously monitoring the seismic activity along this region. Information from this network has revealed that the seismic activity occurs principally in the interior of La Paz Bay and on the coast in front of Isla Cerralvo.

In this article we discuss important issues regarding earthquake ground-motion predictive relations; some of these issues are under active discussion, and others require clarification in terminology or physical interpretation. For example, consider the following.

- Formally speaking, the geometrical spreading factor, $g(r)$, is the decrease in wave amplitude with source due to the increase in area of the wavefront and the law of conservation of energy. However, in practice, this factor takes into account both geometrical spreading and frequency-independent wave-propagation effects when used to represent time-domain amplitude (Yang, 2002). This effective geometrical spreading factor apparently varies with depth (Frankel, 1991) or scattering (Gagnepain-Beyeneix, 1987). The geometric decay depends on the refraction of the direct wave at the upper layer above the hypocenter; therefore, it is strongly dependent on depth. In addition, there is a question whether geometrical spreading varies with frequency. Also, values that decay faster than $1/R$ (e.g., $1/R^{1.2}$) have been reported previously (Malagnini and Herrmann, 2000; Bay *et al.*, 2003; Drouet *et al.,* 2005), but the physical interpretation varies.
- Anelastic attenuation, $Q(f)$, is measured in several ways. Some methods are based on *S*- or *P*-wave maximum amplitudes, whereas others are based on coda characteristics. Estimations of anelastic attenuation depend on the method applied since there is a trade-off between geometrical

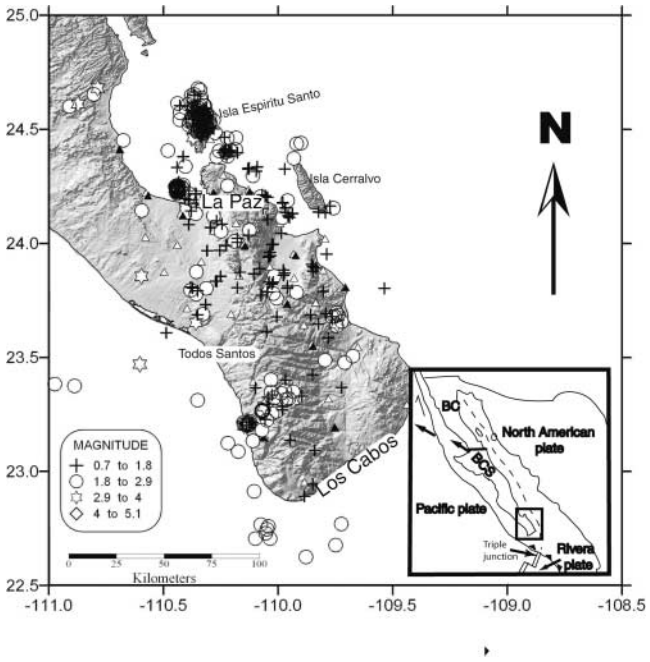

Figure 1. Location of the La Paz–Los Cabos study area within Baja California Sur, Mexico. Open triangles represent digital stations; filled triangles show the location of the analog stations. These analog stations were used only for location purposes. Most earthquakes are located in the La Paz Bay and in the surrounding islands.

spreading and $Q(f)$. In this article we test the *S*-wave and coda shape methods to compare them.

- Small earthquakes are related to large earthquakes via scaling laws, which in turn depend on scalar moment and a stress parameter, assuming that the stress parameter is constant over a studied region. The main idea of scaling laws is that the size of the earthquake increases proportionally with length, width, and final dislocation, assuming that the physics of failure is identical for large and small earthquakes. This physical relation, namely self-similarity, implies that the stress parameter should be independent of earthquake size because it is proportional to fault displacement divided by its length. In fact, it is widely accepted that self-similarity exists for moderate earthquakes. However, there is a question whether self-similarity is valid for small earthquakes (Abercrombie, 1995) or whether it varies with lower magnitudes (e.g., Archuleta *et al.*, 1982; Shi *et al.*, 1998).
- Most methods require a reference distance, but these distances may have different interpretations. In some cases the reference distance ($R_0 \sim 1$ km) is that in which the energy is liberated, and after that the form of the attenuation is known, whereas others are related to observation distances. A good example for observation distance is the local magnitude estimation, assuming that a magnitude 3 earthquake should record a maximum peak of 1 mm on a Wood–Anderson seismogram when recorded at a distance of 100 km.

In this article we quantify the source parameters, attenuation, and site amplification using data of the Red Sísmica de La Paz (LAP) strong-motion network. During the period of 1997–2005, LAP recorded more than 452 useful events; all of them were low-magnitude earthquakes ($M_w < 3.6$). The methodology used in this work consists of a linear regression of the maximum-velocity amplitude logarithm in the time and frequency domains.

Method

The digital data are corrected for instrument response to ground velocity in meters per second, and each waveform is filtered with an eight-pole bandpass Butterworth filter. The center frequencies used are $f_0 = 1.7$, 2, 3, 4, 5, 6, 7, 8, 9, and 10 Hz, and the low- and high-corner frequencies are $f_0 \cdot (1/\sqrt{2})$ and $f_0 \cdot \sqrt{2}$, respectively. The lowest frequency of 1.7 Hz was chosen because it is the minimum frequency that had robust results. In addition to the time-domain Butterworth filter, we computed the Fourier velocity spectrum, and used the frequency windows between the corner frequencies of the bandpass filters to compute the maximum ground-motion spectral level. The signals were transformed by an fast Fourier transform (FFT) routine, smoothed by a 1/8-band filter, and 3% tapered. This two-domain analysis is performed only for completeness since the signals should be similar, and we expect no difference between time and frequency domains.

The observed logarithm of the measured ground motion, $A(r, f)$, of the peak filtered or Fourier velocity is modeled at each frequency by a general regression equation:

$$\log A_{ij}(r, f) = E_i(r_{\text{obs}}, f) + \text{SITE}_j(f) + D(r, f), \quad (1)$$

where r is the hypocentral distance, i is the source index ($1 \le i \le I$), j is the site index ($1 \le j \le J$), $E_i(r_{\text{obs}}, f)$ is the excitation term, and $\text{SITE}_j(f)$ represents the site term. $D(r, f)$ is a piecewise linear function (Yazd, 1993; Anderson and Lei, 1994; Harmsen, 1997) used to represent the distance dependence at a fixed frequency, f:

$$D(r, f) = \sum_{k=1}^{n} L_k(r) D_k, \quad (2)$$

where n is the number of nodes, $L_k(r)$ is a linear interpolation function, the $D_k = D(r_k, f)$ are node values, and r_k is a fixed distance chosen to give a good sampling in the log space in such a manner that sufficient observations lie within each pair of nodes. This linear system can be solved by a least-squares inversion using a singular value decomposition algorithm (Lawson and Hanson, 1974). The following constraints are used in this study to reduce the number of

degrees of freedom of the system to permit a stable inversion: (1) $D(r_{obs}) = 0$, where $r_{obs} = 40$ km; (2) $\Sigma\ \mathrm{SITE}_j(f) = 0$; and (3) a smoothing constraint applied to the $D(r)$, $D_{k-1} - 2D_k + D_{k+1} = 0$ (Malagnini *et al.*, 2000).

As a check on the regression, we applied the coda-normalization technique (Aki, 1980; Frankel *et al.*, 1990) to provide an independent estimate of the $D(r, f)$, which should be independent from instrument response and unknown source and site effects, as long as these values do not change with time. Once the regression was performed, we modeled the excitation and distance terms by comparing predicted Fourier velocity spectra and $D(r, f)$ with the observed functions. An equation for the predicted Fourier velocity spectra at a frequency f observed at a hypocentral distance r_{obs} follows:

$$E(r_{obs}, f) = \log[S(f, M_w)] + \log\left[g(r_{obs})\exp\left(\frac{-\pi f r_{obs}}{Q(f)\beta}\right)\overline{V}(f)e^{-\pi f k_{eff}}\right], \quad (3)$$

where $S(f, M_w)$ is the source Fourier velocity spectrum, M_w is the moment magnitude, $g(r_{obs})$ is the geometrical spreading function relative to 40 km, $Q(f)$ is the frequency-dependent quality factor, $\overline{V}(f)$ is a site-amplification function, β is the shear-wave propagation velocity, and k_{eff} is a site-attenuation coefficient. The second term propagates the $S(f, M_w)$ to distance $r_{obs} = 40$ km.

We used a simple ω^2 model as $S(f)$ (e.g., Anderson and Hough, 1984):

$$S(f) = \frac{CM_0 2\pi f}{1 + (f/f_c)^2}, \quad (4)$$

where C is equal to $(0.55)(2)(0.707)/4\pi\rho\beta^3$, 0.55 is the average radiation pattern ($R_{\theta\phi}$), the factor 2 corresponds to the free-surface amplification, 0.707 is the energy partitioning in the two horizontal components, ρ is density, β is the average shear-wave crustal velocity (3.5 km/sec), f_c is the corner frequency related to the radius of the circular source (r_s) by:

$$f_c = \frac{0.37\beta}{r_s}. \quad (5)$$

On the other hand the seismic moment M_0 is related to r_s by (Brune, 1970):

$$M_0 = \frac{16}{7}\Delta\sigma r_s^3 \times 10^{-6} \quad (6)$$

Combining equations (5) and (6) leads to:

$$f_c = 4.8 \times 10^6 \beta\left(\frac{\Delta\sigma}{M_0}\right)^{1/3}, \quad (7)$$

where $\Delta\sigma$ is the stress parameter in bars. M_0 is the scalar seismic moment in dyne cm, which in turn is related to the moment magnitude by (Kanamori 1977):

$$M_w = \left(\frac{\log M_0}{1.5}\right) - 10.73. \quad (8)$$

The combination of equations (4), (7), and (8) are in fact the $S(f, M_w)$ of equation (3). In addition, $D(r, f)$ is parameterized using the following formula:

$$D(r, f) = \log\left[g(r)\exp\left(\frac{-\pi f r}{Q(f)\beta}\right)\right] - \log\left[g(r_{obs})\exp\left(\frac{-\pi f r_{obs}}{Q(f)\beta}\right)\right]. \quad (9)$$

The first term of equation (7) controls the shape of the attenuation curve. On the other hand, the second term is a scalar that only adjusts the level of reference to the observation distance r_{obs}. Note that if $r = r_{obs}$, then $D(r, f) = 0$.

In this study we regress the peak values of bandpass-filtered waveforms of the recorded time histories, the filters being defined around a set of central frequencies. Filtered velocities are used instead of the usual peak motion or response spectra because we preferred to separate the contribution of different frequencies. We observe and parameterize narrow bandpass-filtered ground velocities in the context of the random vibration theory (RVT [Cartwright and Longuet-Higgins, 1956]). Boore (1983) showed that the RVT model is quite robust in predicting the standard engineering ground-motion parameters. RVT allows the prediction of the extrema of time histories if their spectral moments are known. It follows that the parameters obtained from the analysis of the peak-filtered velocity can be used for predicting other quantities of engineering interest, such as the peak ground acceleration, the Fourier amplitude spectra, or the response spectra. The quantification of an effective duration of the seismograms as a function of hypocentral distance and frequency is critical for a correct use of RVT (Malagnini, 1999; Raoof *et al.*, 1999).

In general, a geometrical spreading of $g(r) = r^{-1}$ should be applicable at short distances (<40 km) since it is the spherical spreading of the body waves, but stronger decay has been reported, especially for low frequencies. Since we never have observations at the source, this geometrical spreading function is used in combination with $Q(f)$ to model the excitation instead of modeling the source spectra directly. The source spectra are extrapolated to r_{obs} from the source itself.

Data

The seismic data set was recorded with 10 digital three-component accelerographs and 6 analog seismographs. The

analog seismograms were used only for location purposes. Six digital stations were equipped with Kinemetrics Altus K2 recorders and Epi-sensor accelerometers (FBA ES-T). The other four consisted of K2 accelerographs with internal force-balanced sensors (FBA-23). The digital instruments were set to record ground-acceleration amplitudes of up to 0.5 g at a rate of 200 samples/sec. The analog stations consisted of vertical-component Kinemetrics seismometers (Ranger SS-1) of a 1-sec natural period coupled to Sprengnether seismographs (MEQ-800B).

At the initial stage of the project, only five analog stations were operated in the northern part of the study area. Later, the digital accelerographs initiated operation and recorded the seismicity that occurred in the neighborhood of La Paz. Despite the field work being performed on an irregular temporal basis, a continuous microseismic activity was observed in the aftershock zones of the June 1995 La Paz earthquakes.

The original purpose of this network was to monitor the microseismic activity of the entire La Paz–Los Cabos region. After some time of operation with the first network, most of the stations were removed and reinstalled in a new area. This process of reassigning and removing stations was repeated during the 5-year period of recording. Each time, the network recorded from 5 months to more than 1 year, depending on the seismic activity of each area. Station locations are described in Table 1.

Acceleration waveforms were recorded for microearthquakes with moment magnitudes of up to 3.6. Since most of the digital data correspond to events of small magnitudes, however, the peak amplitudes on the waveforms are of the order of a few centimeters per seconds squared. The regression was performed following the multiple linear analysis described earlier. First, the corrected ground acceleration is integrated to obtain the velocity time history and then is processed in the time and frequency domains. The next step of our analysis was to apply the regression analysis to the maximum filtered bandpass or Fourier amplitude.

We present results for $D(r, f)$ in Figure 2. As expected, bandpass and Fourier amplitude results are similar. Figure 3 presents the distance distribution for each station. In practice we need to cover a wide range of distances and overlap with other stations. We observe that the bulk of data is between 6 and 80 km, however; in general, the coverage is good up to 180 km.

In addition, we computed the S wave as follows; starting from the S-wave arrival time of the filtered velocity, the waveform is squared and integrated. Then, the integrated energy is normalized to a unit maximum value, and the time between 5 and 75% of the integrated energy is computed. The duration time for each frequency is plotted in Figure 4. We observe that for frequencies higher than 5 Hz, durations are very similar. We used vertical (Z) only and horizontal (H) and vertical components with site constraints $\Sigma\ \mathrm{SITE}_Z = 0$, and $\Sigma\ \mathrm{SITE}_H = 0$ and we found no difference between both data sets.

Coda Normalization

Aki (1980) proposed a coda-normalization approach for measuring the amplitude attenuation of direct S waves with travel distance in the lithosphere. Aki's (1980) method has become known as the coda-normalization method, and has been successfully demonstrated to be a powerful tool to estimate the quality factor Q_s^{-1}. In this method the amplitude of the peak motion is divided by the coda level to eliminate or minimize the instrument gain, source excitation, and site-amplification effects. Figure 5 (top) indicates the attenuation curve for different frequencies based on the coda-normalization method. In the figure the coda normalized levels are represented as the "raw" data (plusses). We presented these "raw" data as the coda piecewise linear function (gray line) using equation (2) to compare the coda normalization with $D(r, f)$.

The coda-normalization method provides a reliable way to estimate the distance dependence of ground motion, eliminating the influence of source and site amplification and isolating the propagation term. This method is based on the assumption that the coda energy is uniformly distributed in the region surrounding the source. Consistency of the results obtained by the coda-normalization method helps to confirm the validity of the assumption. A key observation supporting coda normalization is that for local earthquakes recorded at distances where arrival times are greater than twice the travel time of an S wave from a source to a receiver, the envelope of a bandpass-filtered seismogram has a common shape that is independent of the source–receiver distance. The amplitude of the envelope varies with source size and recording site amplification.

Coda normalization works best when the peak motion part of the seismogram includes contributions from many rays, as expected at distances much greater than the source depth, and if both coda and peak motion sample similar paths of the focal sphere. Both assumptions are most likely valid for the shallow events used in this study (depth < 16 km). The $D(r, f)$ term from the coda analysis is not used for forward modeling, but only as a comparison. Figure 5 compares the coda-normalization technique and the general linear regression. In general, we observe good agreement in both analyses, especially for low frequencies. At frequencies higher than 4 Hz the coda-normalization curve decays faster than the general linear-regression curve, especially at distances greater than 80 km. At these distances, no more than two stations recorded the same event because the earthquake sizes are small; therefore, the azimuthal coverage is limited. The signal-to-noise ratio of these events is low ($\mathrm{xrms}_{\mathrm{ppi}} < 4 \cdot \mathrm{xrms}_{\mathrm{noise}}$, where $\mathrm{xrms}_{\mathrm{ppi}}$ and $\mathrm{xrms}_{\mathrm{noise}}$ are the rms Fourier amplitude spectra before and after the p arrival, respectively). Therefore, it appears that the coda normalization is not so accurate at these distances because of the limitation of the data set. In general, however, the coda normalization is a good approximation for the attenuation curves.

Table 1
Seismic-Station Characteristics

Station Name	ID	Latitude (N)	Longitude (W)	Lithology
La Presa de la Buena Mujer	PRE	24°05.34′	−110°11.63′	Weathered granite
Cerro del Puerto	CEP	24°04.05′	−110°06.62′	Weathered granite
Isla Partida	IPA	24°33.99′	−110°24.00′	Tuffs
Isla Espíritu Santo	IES	24°27.39′	−110°18.31′	Weathered granite
Rancho Las Vinoramas	VIN	24°11.60′	−110°12.52′	Alluvium
Rancho El Saltito	SLT	24°14.14′	−110°08.37′	Granodiorite
Rancho Cajón de los Reyes	CLR	24°13.25′	−110°35.17′	Alluvium
Rancho San Ramon	RSR	24°03.29′	−110°17.64′	Alluvium
CIBNOR	CIB	24°07.74′	−110°26.13′	Alluvium
Rancho El Coyote	COY	24°17.89′	−110°15.03′	Conglomerate
Ejido Alvaro Obregón	ALO	23°51.51′	−110°10.83′	Gabro
Rancho San Isidro	RSI	23°59.82′	−110°09.61′	Weathered granite
Rancho Tecuan	TEC	23°50.94′	−109°56.47′	Weathered granite
Rancho Boca del Alamo	BDA	23°52.96′	−109°48.83′	Weathered granite
Ensenada de Muertos	EDM	24°01.18′	−109°48.34′	Sandstone
Ejido El Sargento	ESA	24°05.20′	−110°00.11′	Weathered granite
San Antonio	SAN	23°48.35′	−110°03.85′	Weathered granite
San Bartolo	SBA	23°44.39′	−109°50.84′	Weathered granite
Rancho Los Paredones	RLP	23°38.48′	−109°53.95′	Weathered granite
Rancho La Ballena	RLB	23°44.60′	−109°58.58′	Weathered granite
Buena Vista	EBV	23°39.34′	−109°42.84′	Conglomerate
Rancho San Dionisio	SND	23°33.46′	−109°51.91′	Conglomerate
Rancho El Ciruelón	REC	23°41.44′	−110°12.97′	Alluvium
Ejido El Carrizal	EEC	23°47.38′	−110°19.06′	Alluvium
Rancho La Virgencita	RLV	24°01.59′	−110°35.32′	Alluvium
Rancho Los Altares	RLA	23°52.43′	−110°30.42′	Alluvium
Caduaño	CAD	23°19.07′	109°47.47′	Conglomerate
Ejido El Pescadero	PES	23°23.56′	−110°07.15′	Granite
Rancho El Manglito	MAN	22°57.17′	−109°53.76′	Weathered granite
Potrero San Pedro	PSP	23°55.25′	−110°20.71′	Alluvium
San Juan de la Costa	SJC	24°22.26′	−110°41.01′	Alluvium
CICESE	CIC	24°07.72′	−110°18.42′	Alluvium

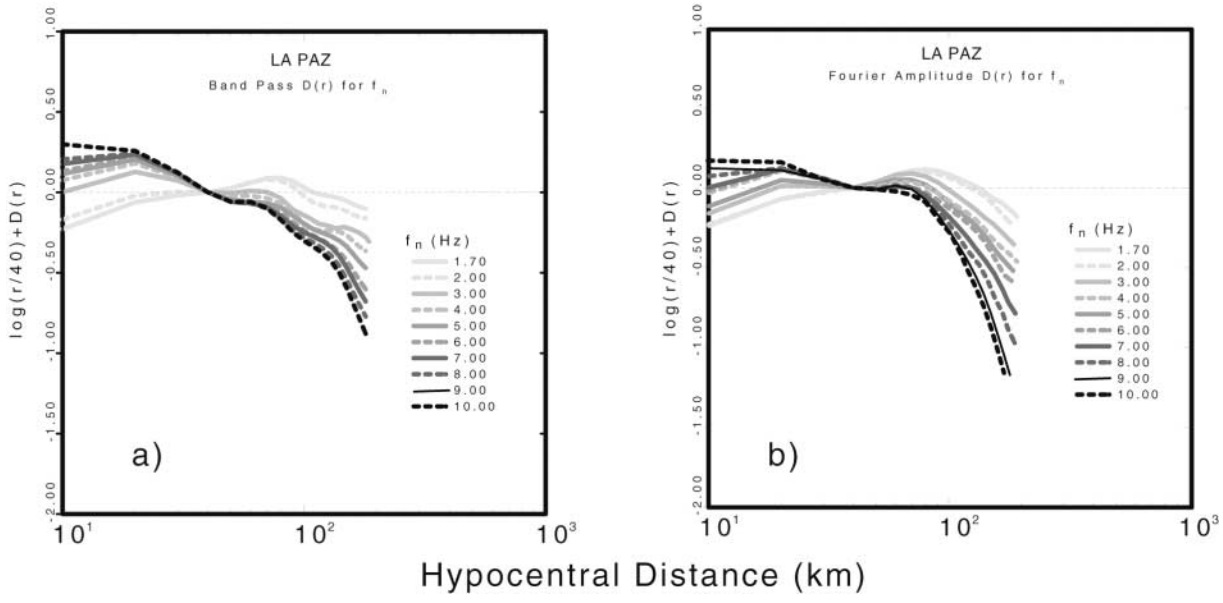

Figure 2. Regression results for $D(r, f)$: (a) bandpass-filtered and (b) Fourier amplitudes. The $D(r, f)$ measurements are inverted from the combined vertical and horizontal data sets. In general, they are similar to each other, but the Fourier amplitude $D(r, f)$ decays slightly faster than the bandpass-filtered amplitude.

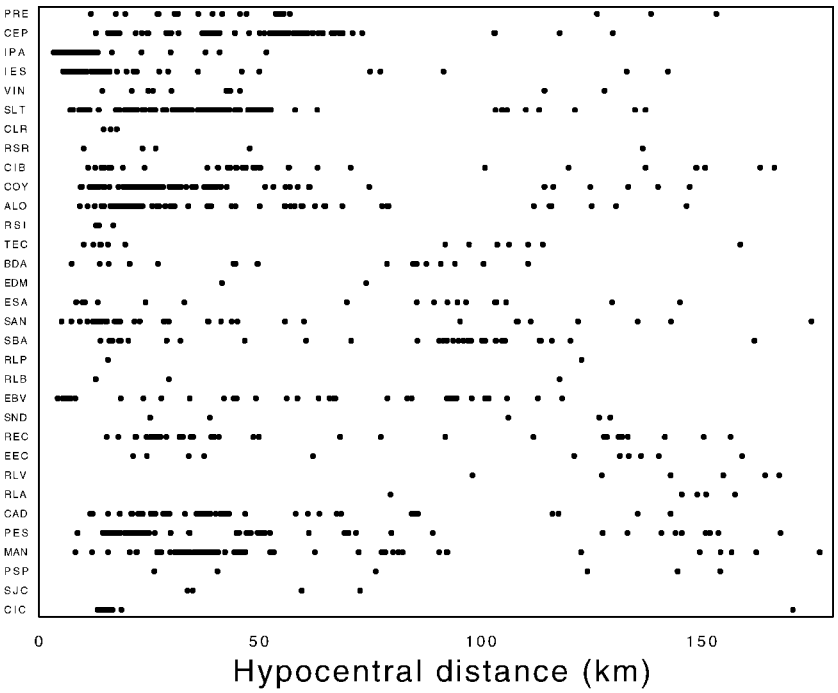

Figure 3. Distance coverage for LAP stations. The hypocentral distances for each station should cover a wide range, overlapping other stations to avoid a trade-off between propagation and excitation.

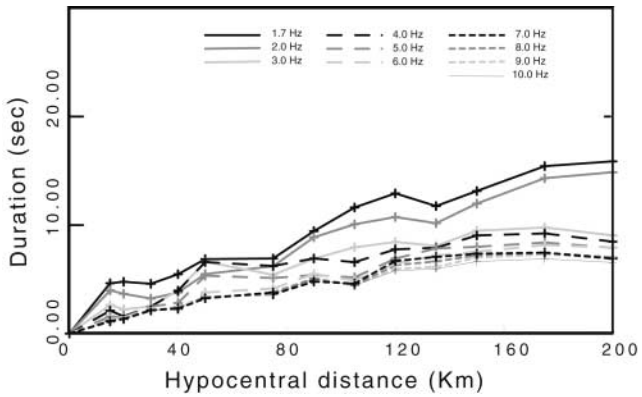

Figure 4. Duration times obtained at different frequencies. For frequencies higher than 5 Hz, duration times are very similar. These values were used for RVT prediction.

RVT Models

In Figure 6 we compare the regression results for bandpass-filtered velocity with two proposed models. We used equation (9) via RVT as coded by Boore (1996) to predict the maximum ground-motion level. The parameters of each model are described in Table 2. We compared these two models to illustrate the nonuniqueness of the attenuation curves if only $D(r, f)$ is considered independent of the excitation terms. The fast-decaying model (HIGHAT) represents a high seismic-wave attenuation model, whereas the second model (LOWAT) has low-attenuation characteristics. Both models apparently match well with the observed attenuation curves; HIGHAT is in better agreement with the high frequencies, whereas LOWAT compares better with the low frequencies.

This example illustrates that it is not possible to parameterize $D(r, f)$ correctly using only the distance term without considering the excitation levels. Moreover, at the beginning of this study we were biased to choose the HIGHAT model ($Q(f) = 180\, f^{0.32}$) since previous observations of the attenuation curve apparently are in better agreement with those of southern California (González *et al.*, 2006). Note that Raoof *et al.* (1999) estimated a $Q(f) = 180\, f^{0.45}$ in southern California using virtually the same technique, but it is necessary to compare the excitation levels to assign values for $Q(f)$ and $g(r)$.

On the other hand, González *et al.* (2006) found that positive M_L station corrections correlate well with hard-rock sites, whereas negative corrections correlate with soft or sedimentary rock sites. We found results similar to those of González *et al.* (2006) for the site term because we used the same data. In addition, Escobar (2004) found site amplification in four stations located on alluvium by using a spectral ratio method (H/V). A detailed study of site amplification is beyond the scope of this study.

Source Excitation

To scale the excitation levels, it is necessary to estimate the magnitude of the earthquakes. We compared the observed and predicted $E(r_{obs}, f)$ of events with known M_w. Recently, Munguía *et al.* (2006) estimated the moment magnitude M_w of the events used in this study. In addition, González *et al.* (2006) computed the local magnitude attenuation parameters ($\log A_0$). It has been widely recognized that for

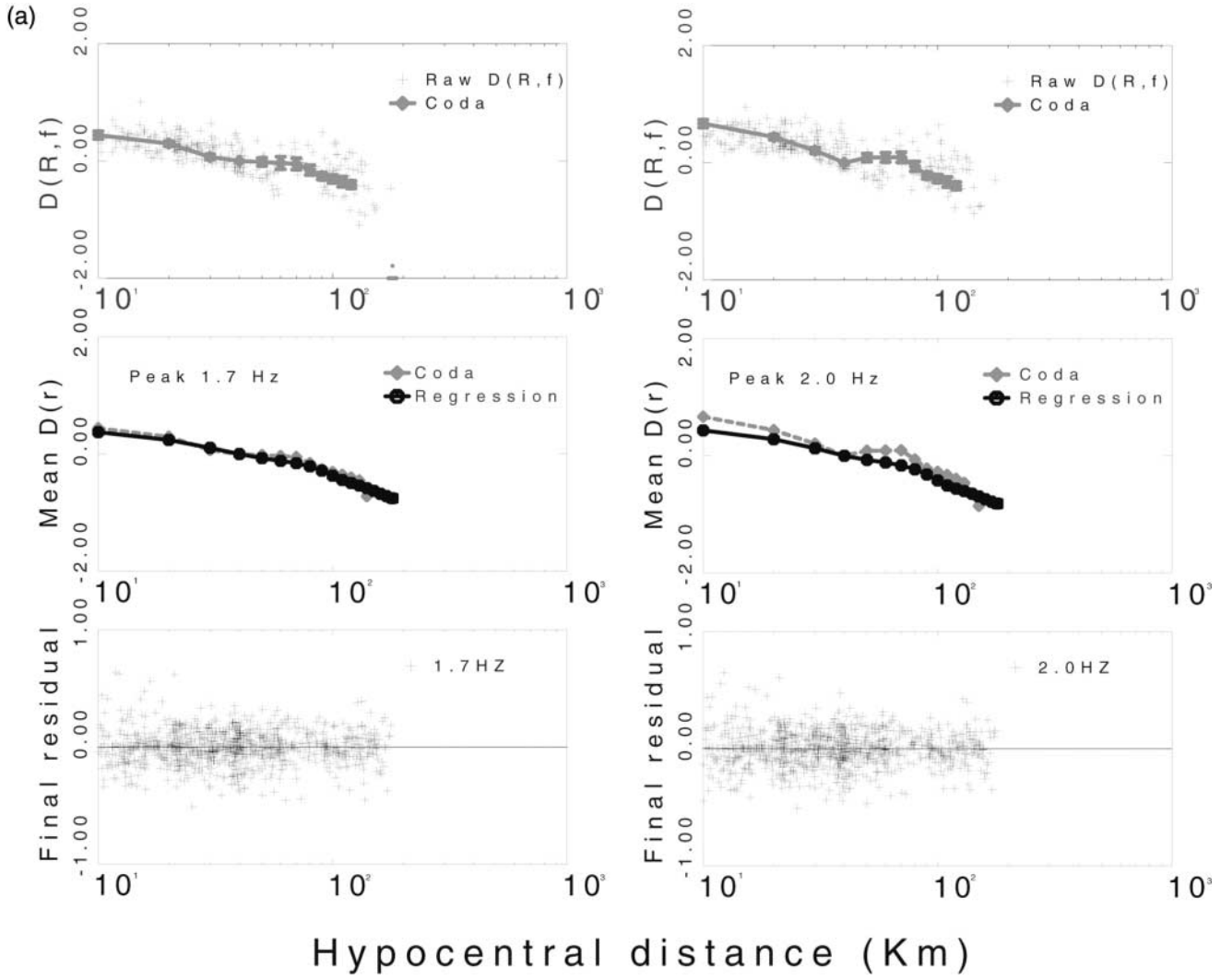

Figure 5. Time-domain regression results. (a) $D(r)$ using the coda-normalization technique. The coda-normalized levels are represented as the "raw" data (plusses). The coda function (gray line) is a piecewise linear function obtained from the regression of the raw data using equation (2). (b) Comparison of coda normalization and general linear regression. (c) Final residuals of the general regression analysis. (*continued*)

small earthquakes (M_w <4.0) the moment magnitude agrees well with the M_L. Munguía *et al.* (2006) observed that this case was not an exception and that most of the calculated magnitudes differed in the worst case by no more than 0.4 units.

We used as a comparison the moment magnitude reported by Munguía *et al.* (2006). The seismic moment was obtained via standard spectral analysis of the *S*-wave horizontal signals. In Figure 7 we present the $E(r_{obs}, f)$ at 40 km from the source. We compared the two models of the preceding section. First, we tested the HIGHAT model (Table 2). This model apparently has similar attenuation characteristics to those of southern California based on the shape of the attenuation correction of the local magnitude (log A_0 [González *et al.*, 2006]). However, we could match neither the excitation levels of the M_w 3.6 earthquakes nor the shape of the source spectra translated to 40 km (Fig. 7). The second model, LOWAT, was also tested. We found that LOWAT matched better with the observed excitations. In the next section we discuss the comparison of these two models in more detail.

Discussion and Results

Compared with other regions such as central or northern Mexico (Vidal and Munguía, 1999; Ortega *et al.*, 2003; Ortega and Quintanar, 2005), La Paz–Los Cabos is characterized by a relatively low rate of seismicity. LAP recorded surprisingly high-quality data from low-magnitude background seismicity (Munguia *et al.*, 2006); most of the

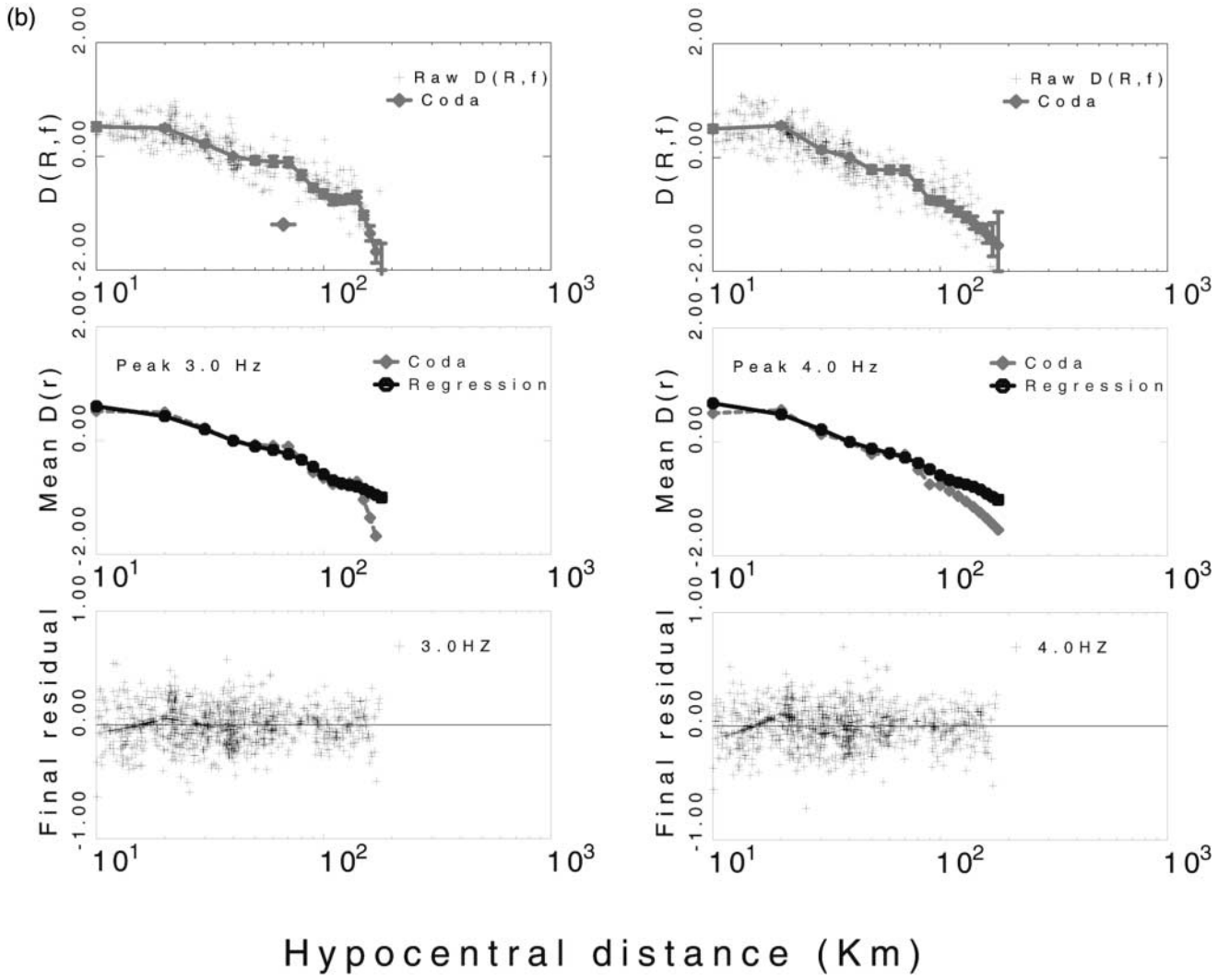

Figure 5. Continued.

earthquakes were recorded at epicentral distances in the range of 6–100 km, and the average magnitude was M_w 2.5.

A striking observation is that we obtained more robust results with a strong-motion network than those obtained in central Mexico with a weak-motion network (Ortega and Quintanar, 2005), despite the maximum earthquake magnitude difference in the data sets. Although the central Mexico weak-motion network recorded events up to M_w 5.2, the LAP network only recorded events up to M_w 3.6. In the 7-year period of both networks, LAP recorded more useful events than the central Mexico weak-motion network. LAP started operation 2 years after the 1995 (M_s 6.2) earthquake; therefore, no aftershocks were recorded. These high-quality data are partly due to the earthquake ground-motion characteristics; some other factors such as noise levels at the stations and the distance range of the sources were considered by Munguía *et al.* (2006), but it is necessary to consider other factors such as the amount of time the networks were functioning properly. In addition, cultural noise is higher in central Mexico than in Baja California Sur; these regions are the most and least densely populated areas of the country of Mexico, respectively. Our overall results suggest that seismic-wave attenuation is low compared with that of southern California, Baja California, or central Mexico.

Contrary to expectations, the propagation of seismic waves in Baja California Sur appears to be very different from that of waves traveling in the northern part of the peninsula or in California. Different propagation effects and crustal characteristics have been observed along the Baja California peninsula. For example, on the basis of only sparse measurements, the heat flow values for the Baja California peninsula range from 42 to 84 mW/m^2 (Urrutia-Fucugauchi, 1986) compared with those of about 92 mW/m^2 in central Mexico (Ziagos *et al.*, 1985). On the other hand, crustal thickness along the Baja California peninsula appears to be uncorrelated with topography (Persuad, 2003). The Moho beneath the Peninsular Ranges is not flat, however, nor is the crustal thickness anticorrelated with crustal

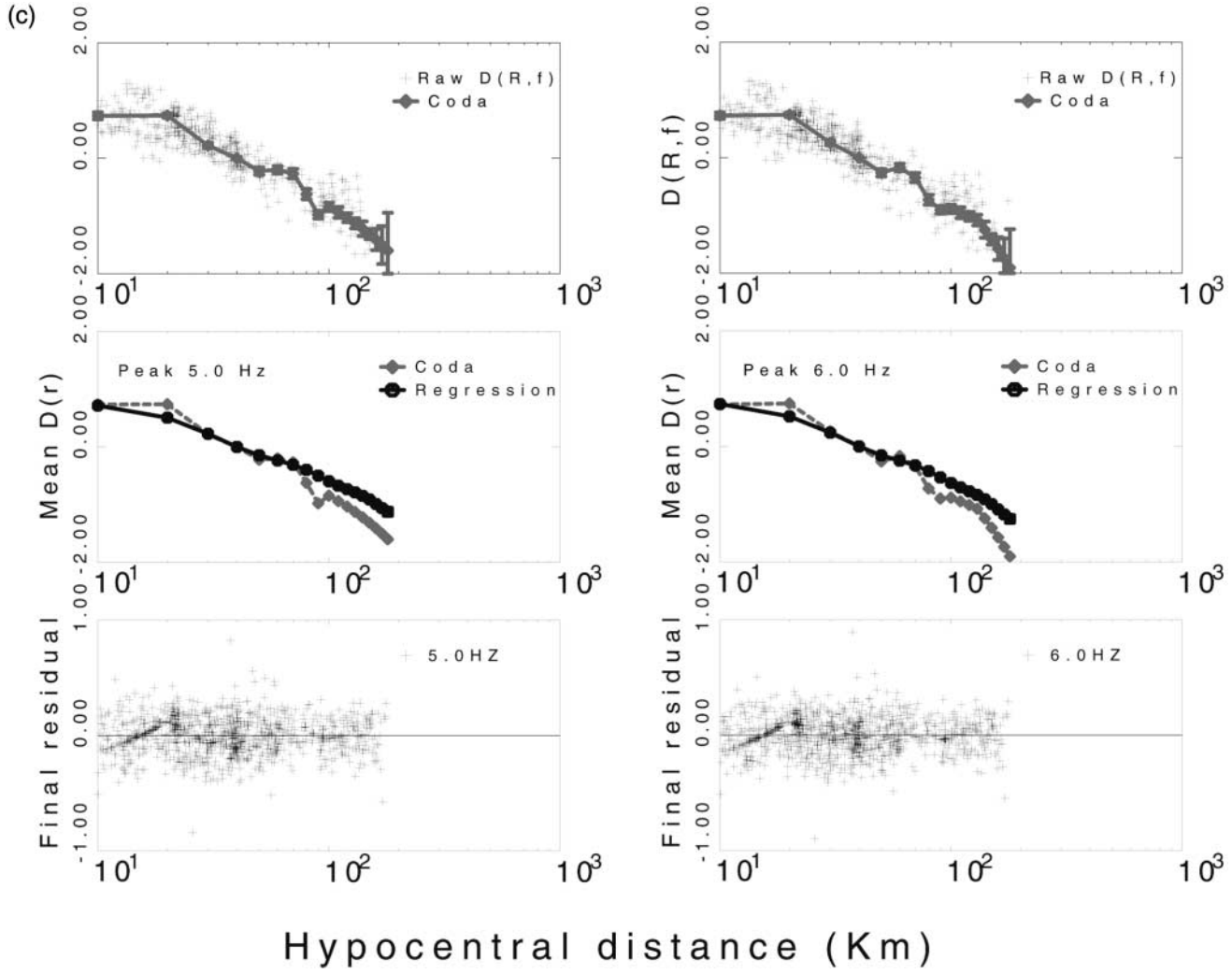

Figure 5. Continued.

density, as in the southern Sierra Nevada (Wernicke *et al.*, 1996).

The flattening of $D(r)$ between distances of 50 and 90 km (40 and 70 km) (Fig. 5) is attributed to critical reflections of the shear waves from the Moho. This feature is observed at low frequencies (<5 Hz). These "bumps" are modeled in the parametric form in the geometrical spreading function, $g(r)$, that controls some changes in seismic-wave propagation. Another explanation for this low value of the exponent of distance in the geometrical spreading term is the interaction between body- and surface-wave fields. In both models of table 2 the geometrical spreading factor after 100 km is $1/R^{0.5}$, suggesting that *Lg* waves are the prominent part of the wave field between 100 and 180 km. In this work, faster decay than $1/R$ of the geometrical spreading does not necessarily describe reflections of the direct waves at the base of the layer above the focus, as described by Frankel (1991), but model elastic propagation effects on amplitudes along the seismic-wave travel path.

Scaling laws are functions that express the corner frequency in terms of the stress parameter and the scalar moment M_0 (Brune, 1970). Since source models (e.g., ω^2 model) predict the source spectra based on corner frequencies, the scaling law is a powerful tool for predicting the source excitation of big earthquakes from small earthquakes, assuming that the stress parameter is constant over a studied region. However, some authors argue that the stress parameter is not always constant over a large-magnitude range (e.g., Mayeda and Walter, 1996; Ide and Beroza, 2001). The question is whether this parameter, although it is still called "stress drop" against convincing arguments (Atkinson and Beresnev, 1997), should be considered independent of magnitude. In this work we considered a constant stress drop over magnitude; this assumption is valid since our magnitude range is small (M_w 2.0–3.6) and we did not record any moderate events (M_w >5.5). Moreover, for M_w 2 there is a little dependence on the shape of the spectrum between 1 and 16 Hz as a function of the stress parameter (Jeon and

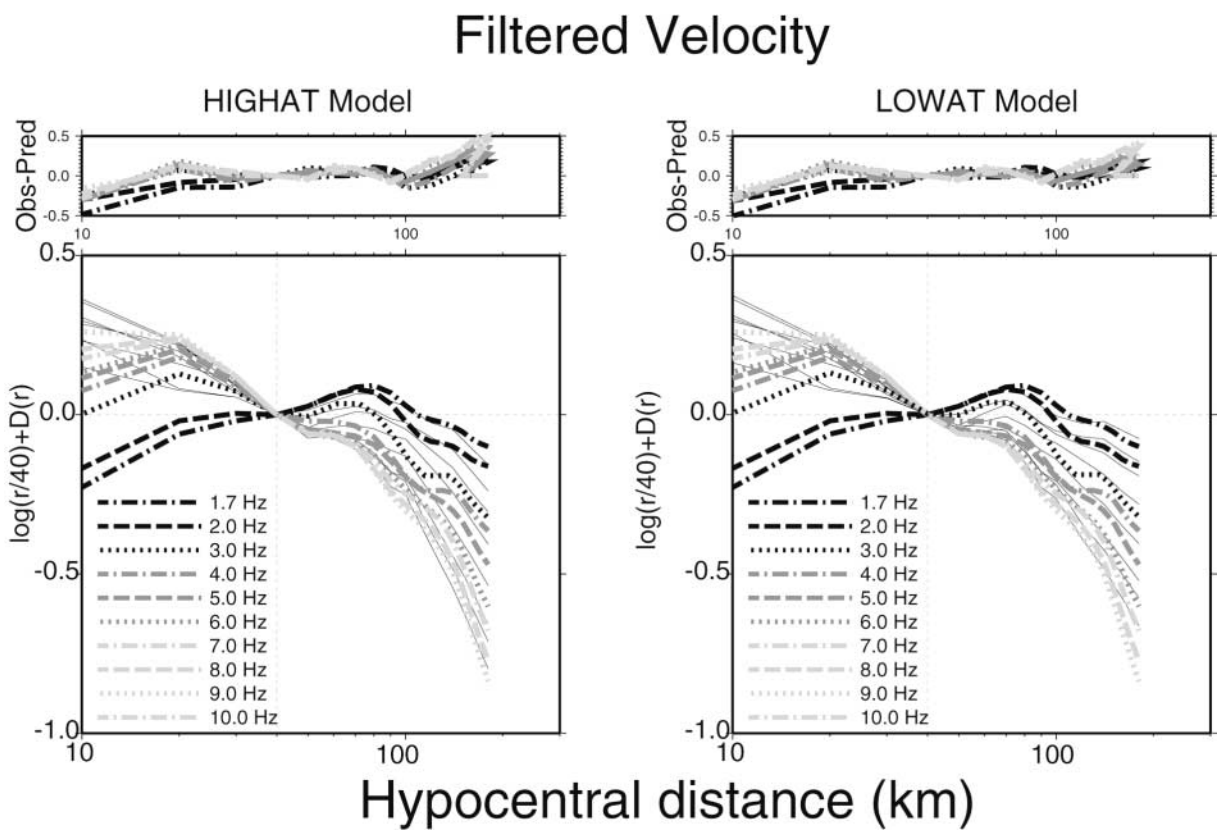

Figure 6. Final regression and RVT models for the filtered time domain $D(r)$. Discontinuous lines correspond to the general regression, and the thin lines are the RVT models. The residual (observed − predicted) is plotted at the top.

Table 2
Attenuation Models

	HIGHAT	LOWAT
κ_{eff}	0.060	0.016
$Q(f)$	$180f^{0.32}$	$380f^{0.10}$
β	3.5	3.5
ρ	2.8	2.8
$g(r)$	$\begin{cases} r^{-1.0} & 0 < r \leq 40 \\ r^{-0.2} & 40 < r \leq 100 \\ r^{-0.5} & 100 < r \leq 180 \end{cases}$	$\begin{cases} r^{-1.1} & 0 < r \leq 40 \\ r^{-0.3} & 40 < r \leq 70 \\ r^{-0.8} & 70 < r \leq 100 \\ r^{-0.5} & 100 < r \leq 180 \end{cases}$
$\bar{V}(f)$	GEN97*	GEN97*
$\Delta\sigma$	40 bars	40 bars

*Amplification factor for generic rock site (Boore and Joyner, 1997).

Herrmann, 2004). Source spectra will not affect the excitation levels if the stress parameter varies in the range of 10–400 bars for $M_w \sim 2$ earthquakes. This means that the shape of the excitation $E(r, f)$ for earthquakes of $M_w \leq 2$ of Figure 7 depends mainly on $Q(f)$ and k_{eff} and is insensitive to the stress parameter. Because of this insensitivity, we should be able to find robust attenuation results and average site effects without worrying about the source spectrum scaling problems related to the stress parameter. However, from a visual inspection of the excitation levels (Fig. 7), we observe that the shape of the observed excitation term in the M_w 2.0 events is more similar to the HIGHAT model, but in the M_w 2.5 it is closer to the LOWAT. Since the population of the M_w 2.5 events is slightly bigger than that of the M_w 2.0 event we prefer the LOWAT model. Because this observation was not conclusive, we compared the excitation levels of the high-magnitude earthquakes ($M_w \sim 3.6$). Munguia *et al.* (2006) estimated the magnitudes of these high-magnitude earthquakes more accurately than those of the low-magnitude events because they have higher signal-to-noise ratios. Therefore we used those earthquakes for scaling purposes. In Figure 7 we observe that the LOWAT model fits the high-magnitude earthquakes better than the HIGHAT model. Note that the observed and predicted terms of these high-magnitude earthquakes should not have to fit exactly, but should follow the same trend as on the shape of the spectra, because at these magnitudes the spectral shape greatly depends on the stress parameter. In any case, we observed that a constant stress parameter is consistent with our results.

Recently, Jeon and Herrmann (2004) observed different crustal attenuation parameters from Utah and Yellowstone by using almost the same technique. They note that Q values determined by Clowson *et al.* (1989) within the caldera may vary in the range of 40–200, whereas outside the caldera they are greater than 200. In Baja California Sur we have

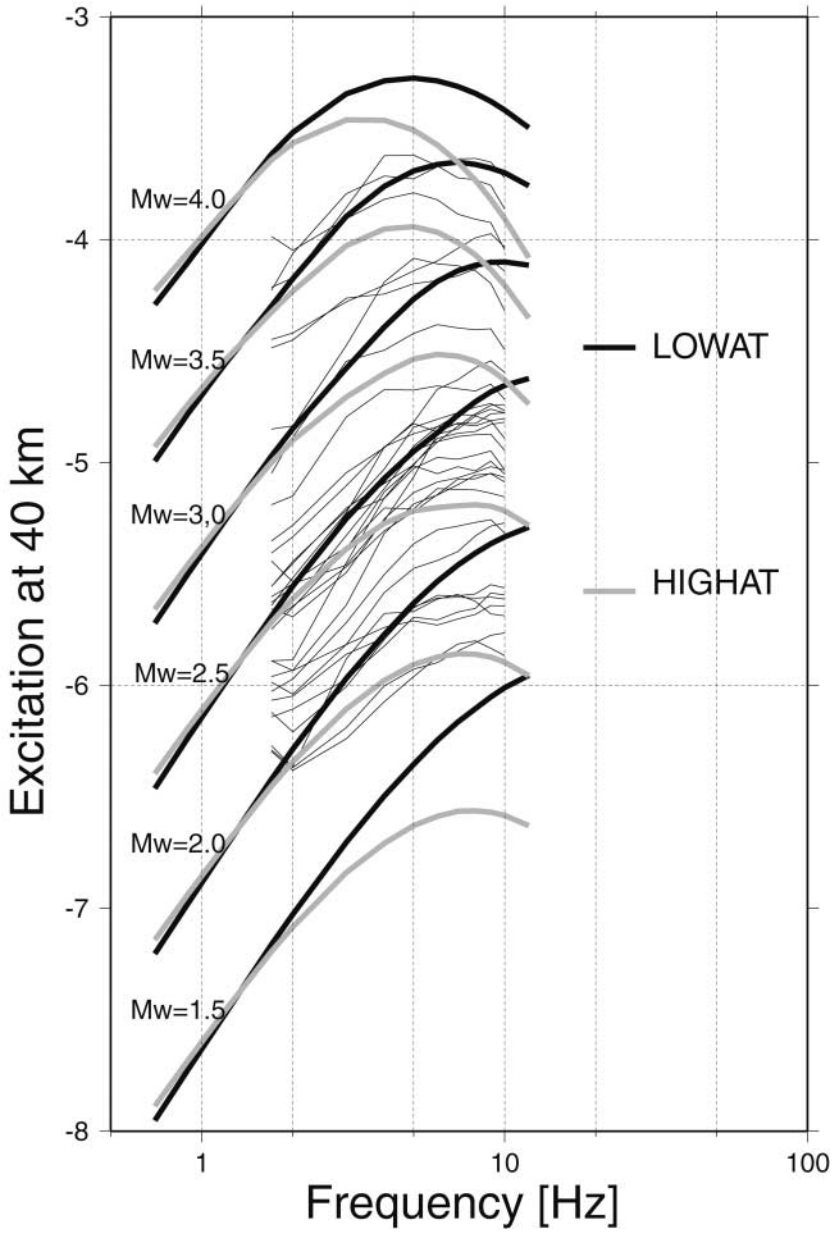

Figure 7. Excitation terms at 40 km from the source. Thin lines correspond to the observed $E(r)$ from the regression. The excitation terms are inverted from the combined vertical and horizontal data sets. The maximum observed earthquake was M_w 3.6. Thick lines are the predicted excitations using RVT. Gray lines correspond to a $Q(f) = 180f^{0.32}$, whereas the black lines correspond to a $Q(f) = 380f^{0.40}$. We presented only a small set of excitation terms to clarify the shape of the spectra.

observed important seismic activity related to volcanic events within Bahia Concepción and Volcán Tres Virgenes, located only 500 km north of La Paz. Future studies within and around the volcanic area will provide information about the attenuation. It has been recognized that thermal, anelastic, and scattering processes affect Q at high frequencies in the crust. Some of the factors that affect the attenuation are heat flow, amount of fluid content, and partial melt in the crust and upper mantle. We believe, therefore, that Baja California Sur has complex seismic-wave attenuation characteristics.

Acknowledgments

We acknowledge Sergio Mayer and Alfredo Aguirre, who diligently maintain the LAP stations. Luis Munguía is warmly thanked for allowing us to use the data. Marco Mucciarelli and an anonymous reviewer provided helpful comments that significantly improved the presentation of this article. The regression analyses were carried out using the ground-motion scaling programs written by Robert B. Herrmann. This article is dedicated to the memory of Cecilio Rebollar who was the pioneer of seismic instrumentation in the Baja California Peninsula. This project was supported in part by CICESE-La Paz and CONACYT-Mexico under grant 46138.

References

Abercrombie, R. E. (1995). Earthquake source scaling relationships from -1 to 5 M_L using seismograms recorded at 2.5-km depth, *J. Geophys. Res.* **100,** 24,015–24,036.

Aki, K. (1980). Attenuation of shear waves in the lithosphere for frequencies from 0.05 to 25 Hz, *Phys. Earth Planet. Interiors* **21,** 50–60.

Anderson, J. G., and S. E. Hough (1984). A model for the shape of the Fourier amplitude spectrum of acceleration at high frequencies, *Bull. Seism. Soc. Am.* **74,** 1969–1993.

Anderson, J. G., and Y. Lei (1994). Non-parametric description of peak acceleration as a function of magnitude, distance and site in Guerrero Mexico, *Bull. Seism. Soc. Am.* **84,** 1003–1017.

Archuleta, R. J., E. Cranswick, C. Mueller, and P. Spudich (1982). Source parameters of the 1980 Mammoth Lakes, California, earthquake sequence, *J. Geophys. Res.* **87,** 4595–4607.

Atkinson, G. M., and I. A. Beresnev (1997). Don't call it stress drop, *Seism. Res. Lett.* **68,** 3–4.

Bay, F., D. Fäh, L. Malagnini, and D. Giardini (2003). Spectral shear-wave ground motion scaling in Switzerland, *Bull. Seism. Soc. Am.* **93,** 414–429.

Boore, D. M. (1983). Stochastic simulation of high frequency ground motion based on seismological models of the radiated spectra, *Bull. Seism. Soc. Am.* **73,** 1865–1894.

Boore, D. M. (1996). SMSIM—Fortran programs for simulating ground motions from earthquakes: version 1.0, *U.S. Geol. Surv. Open-File Rept. 96-80-A*, Menlo Park, California.

Boore, D. M., and W. B. Joyner (1997). Site amplification for generic rock sites, *Bull. Seism. Soc. Am.* **87,** 327–341.

Brune, J. N. (1970). Tectonic stresses and spectra of seismic waves from earthquakes, *J. Geophys. Res.* **75,** 4997–5009.

Cartwright, D. E., and M. S. Longuet-Higgins (1956). The statistical distribution of the maxima of a random function. *Proc. R. Soc. London A.* **237,** 212–223.

Clowson, S. R., R. B. Smith, and H. M. Benz (1989). P wave attenuation of the Yellowstone Caldera from the three-dimensional inversion of spectral decay using explosion source seismic data, *J. Geophys. Res.* **94,** 7205–7222.

Drouet, S., A. Souriau, and F. Cotton (2005). Attenuation, seismic moments, and site-effects for weak-motion events: Application to the Pyrenees, *Bull. Seism. Soc. Am.* **95,** 1731–1748.

Escobar, J. (2004). Espectros locales de diseño sismico para obras civiles en la región de La Paz, BCS, México, *Undergraduate Thesis*, Instituto Tecnológico de La Paz (in Spanish).

Frankel, A. (1991). Mechanisms of seismic attenuation in the crust: scattering and anelasicity in New York State, South Africa, and Southern California, *J. Geophys. Res.* **96,** 6269–6289.

Frankel, A., J. McGarr, J. Bicknell, L. Mori, L. Seeber, and E. Cranswick (1990). Attenuation of high-frequency shear waves in the crust: Measurements from New York State, South Africa, and Southern California, *J. Geophys. Res.* **95,** 17,441–17,457.

Gagnepain-Beyeneix, J. (1987). Evidence of spatial variation of attenuation in the western Pyrenean range, *Geophys. J. R. Astr. Soc.* **89,** 681–704.

Goff, J. A., E. A. Bergman, and S. C. Solomon (1987). Earthquake source mechanisms and transform fault tectonics in the Gulf of California, *J. Geophys. Res.* **92,** 10,485–10,510.

González, M., A. Vidal, and L. Mungía (2006). A M_L scale for the La Paz-Los Cabos Region, Baja California Sur, México, *Bull. Seism. Soc. Am.* **96,** 1296–1304.

Harmsen, S. (1997). Estimating the diminution of shear wave amplitude with distance: application to the Los Angeles, California, urban area, *Bull. Seism. Soc. Am.* **87,** 889–903.

Ide, S., and G. C. Beroza (2001). Does apparent stress vary with earthquake size? *Geophys. Res. Lett.* **28,** 3349–3352.

Jeon, Y. S., and R. B. Herrmann (2004). High-frequency earthquake ground-motion scaling in Utah and Yellowstone, *Bull. Seism. Soc. Am.* **94,** 1644–1657.

Kanamori, H. (1977). Seismic and aseismic slip along subduction zones and their implications, in *Island Arcs Deep Sea Trenches and Back-Arc Basins, Maurice Ewing Series 1*, M. Talwani and W. C. Pitman, III (Editors), American Geophysical Union, Washington, D.C., 162–174.

Lawson, C. L., and R. J. Hanson (1974). *Solving Least Squares Problems*, Prentice Hall, Englewood Cliffs, New Jersey.

Malagnini, L. (1999). Ground motion scaling in Italy and Germany, *Ph.D. Thesis*, St. Louis University.

Malagnini, L., and R. B. Herrmann (2000). Ground motion scaling in the region of the 1997 Umbria-Marche earthquake (Italy), *Bull. Seism. Soc. Am.* **90,** 1041–1051.

Malagnini, L., R. B. Herrmann, and M. Di Bona (2000). Ground motion scaling in the Appennines (Italy), *Bull. Seism. Soc. Am.* **90,** 1062–1081.

Mayeda, K., and W. R. Walter (1996). Moment, energy, stress drop and source spectra of western United States earthquakes from regional coda envelopes, *J. Geophys. Res.* **101,** 11,195–11,208.

Molnar, P. (1973). Fault plane solutions of earthquakes and direction of motion in the Gulf of California and in the Rivera fracture zone, *Geol. Soc. Am. Bull.* **84,** 1651–1658.

Munguía, L., J. Gaitán, V. Wong, and S. Mayer (1992). Microsismicidad en la zona de la falla La Paz, Baja California Sur, México, *Geofis. Int.* **31,** 279–287.

Munguía, L., M. González, S. Mayer, and A. Aguirre (2006). Seismicity and state of stress in the La Paz-Los Cabos Region, Baja California Sur, México, *Bull. Seism. Soc. Am.* **96,** 624–636.

Ortega, R., and L. Quintanar (2005). A study of the local magnitude scale in the Basin of Mexico: mutually consistent estimates of log A_0 and ground motion scaling, *Bull. Seism. Soc. Am.* **95,** 605–613.

Ortega, R., R. B. Herrmann, and L. Quintanar (2003). Earthquake ground-motion scaling in central Mexico between 0.7 and 7 Hz, *Bull. Seism. Soc. Am.* **93,** 397–413.

Persuad, V. (2003). Images of early continental break-up in and around the Gulf of California and the role of basal shear in producing wide plate boundaries, *Ph.D. Thesis*, California Institute of Technology.

Raoof, M., R. B. Herrmann, and L. Malagnini (1999). Attenuation and excitation of three component ground motion in southern California, *Bull. Seism. Soc. Am.* **89,** 888–902.

Shi, J., W. Kim, and P. G. Richards (1998). The corner frequencies and stress drop of intraplate earthquakes in the Northeastern United Stetes, *Bull. Seism. Soc. Am.* **88,** 531–542.

Urrutia-Fucugauchi, J. (1986). Crustal thickness, heat flow, arc magmatism and tectonics of Mexico—preliminary report, *Geofis. Int.* **25,** 559–573.

Vidal, D., and L. Munguía (1999). The M_L scale in northern Baja California, Mexico, *Bull. Seism. Soc. Am.* **98,** 750–763.

Wernicke, B., R. Clayton, M. Ducea, C. Jones, S. Park, S. Ruppert, J. Saleeby, J. J. Snow, L. Squires, M. Fliedner, G. Jirace, R. Keller, S. Klemperer, J. Luetgert, P. Malin, K. Miller, W. Mooney, H. Oliver, and R. Phinney (1996). Origin of high mountains in the continents: The Southern Sierra Nevada, *Science* **271,** 190–193.

Yang, X. (2002). A numerical investigation of Lg geometrical spreading, *Bull. Seism. Soc. Am.* **92,** 3067–3079.

Yazd, M.R.S. (1993). Ground motion studies in the Southern Great Basin of Nevada and California, *Ph.D. Thesis*, St. Louis University.

Ziagos, J. P., D. D. Blackwell, and F. Mooser (1985). Heat flow in southern Mexico and the thermal effects of subduction, *J. Geophys. Res.* **90,** 5410–5420.

Centro de Investigación Científica y de Educación Superior de Ensenada
Unidad La Paz, Miraflores 334 Fracc. Bellavista
La Paz 23050, Baja California Sur, Mexico
ortega@cicese.mx
(R.O.)

Centro de Investigación Científica y de Educación Superior de Ensenada
B. C. Km 107 Carretera Tijuana-Ensenada
Ensenada, Baja California, C. P. 22860, Mexico
(M.G.)

Manuscript received 3 April 2006.